J Mater Sci (2011) 46:5931–5939
DOI 10.1007/s10853-011-5548-y

Corrosion behavior of surface-modified titanium in a simulated body fluid

Julia van Drunen · Baodong Zhao · Gregory Jerkiewicz

Received: 4 February 2011 / Accepted: 6 April 2011 / Published online: 22 April 2011

Abstract We investigate the influence of micro-sandblasting and electrochemical passivation on properties such as corrosion rate and surface roughness, which are important to the biocompatibility of titanium (Ti), using surface analysis techniques and electrochemical measurements. Results of microscopy and surface profilometry experiments reveal roughened but uniform surface topography with an average surface roughness in the 0.87–1.06 μm range, depending on the alternating current passivation voltage applied to the micro-sandblasted samples. Open circuit potential versus time measurements in Hank's Balanced Salt Solution (HBSS, a simulated body fluid) allow determination of the corrosion potential (E_{corr}) and reveal a shift of E_{corr} toward higher values upon passivation, thus pointing to increased corrosion stability. Corrosion rates in HBSS range between 0.049 and 0.288 μm year^{-1} for micro-sandblasted and passivated Ti, as compared to that for the micro-sandblasted and non-passivated surface that is 0.785 μm year^{-1}. Results from this study demonstrate that micro-sandblasting coupled with electrochemical passivation provides a roughened surface with increased corrosion stability and a low corrosion rate in HBSS. Application of this technique to Ti in medical and dental applications may be expected to result in an improvement of biocompatibility.

J. van Drunen · B. Zhao · G. Jerkiewicz (✉)
Department of Chemistry, Queen's University,
90 Bader Lane, Kingston, ON K7L 3N6, Canada
e-mail: gregory.jerkiewicz@chem.queensu.ca

Introduction

Metallic titanium (Ti) is held in high regard in industries where strength, thermal stability, and low susceptibility to corrosion are required. These properties make Ti and Ti-containing alloys suitable materials for the fabrication of components of engines, aircrafts, and marine vessels, both surface and submarine [1]. Titanium and its alloys are also excellent materials for the production of prosthetic, cardiovascular, and orthodontic implants. The medical industry values Ti for its low density, high mechanical strength, good resistance to biocorrosion, low toxicity, and overall biocompatibility [2]. In 1996, the American Dental Association renewed their stance on the use of Ti in dental implants, stating that Ti and its alloys are the preferred materials for subcutaneous implant devices [3].

In the past, the concept of biocompatibility was associated with the lack of undesirable interactions between an implanted material and its host, the human body [4]. Today's definition of biocompatibility encompasses a more comprehensive and progressive view of how an implant should perform and what properties it should possess. In order to achieve desired biocompatibility, it is best to design a material which compliments patient's physiological processes [4]; such a material should not only be accepted by the human body but should also integrate fully and function in a manner that resembles a human body part, thus as mimicking it. Cooperation between the implanted material and its host is ultimately governed by interactions occurring at the interface where the material comes into contact with tissue, bone, or physiological fluids [4]. Therefore, an understanding of the material's interfacial and biocorrosion properties is crucial in the design of a successful implant [5].

When exposed to the ambient conditions, a stable passive layer forms on the surface of Ti which renders the metal more resistant to chemical processes such as corrosion [6]. Certain applications require a stable, non-reactive Ti surface and, therefore, the oxidation is favored and performed in a controlled manner. Oxide layers on Ti can be formed by thermal treatment in an O_2(g)-containing atmosphere and at high temperature ($T > 700$ °C); the process typically produces an oxide film that possesses the rutile crystallographic structure [7]. Because the standard Gibbs energy of formation of TiO_2(s) with a rutile structure has a large negative value ($\Delta_f G° = -888.8$ kJ mol^{-1}) [8], the oxide layer achieves a significant decrease in reactivity and corrosion of the Ti surface. However, to accomplish a thick, compact oxide layer on Ti, thermal oxidation has to be performed for a long time, up to several hours, which translates into a costly and energy-inefficient process [9].

Stable oxide and passive layers on Ti can also be formed under mild electrochemical conditions and typically employ an aqueous electrolyte solution and a direct current (DC) voltage; the process is commonly referred to as DC anodization [7]. In 1996, Jerkiewicz et al. [10] described an alternative process of forming passive layers on Ti that employs an alternating current (AC) voltage (V_{AC}) and an aqueous NH_4BF_4 solution; it yields passive layers that are compact, stable and reveal bright, well-defined colors [6]. Because the coloration originates from constructive thin-layer light interference, iridescence, it is directly related to the passive layer's thickness. The direct relation between the coloration and the applied V_{AC} makes the coloration tunable and even switchable [11]. As the colored passive layer formation is achieved at room temperature and the polarization time (t_{pol}) is only 10 s, the process is easily scalable and energy efficient.

Chemical etching, mechanical polishing, and micro-sandblasting are different methods of pretreating metallic materials and offer further control over the surface morphology and appearance. In the context of biocompatibility, these methods can be used to alter surface roughness and wettability, ultimately affecting the surface's performance in physiologically relevant environments [12]. In the case of colored Ti, surface pretreatments also alter the appearance of the colored passive layers, resulting in matte, shiny, or reflective surfaces [13].

This study focuses on the influence of micro-sandblasting as a pretreatment for electrochemically passivated titanium. Micro-sandblasting was chosen because it is known that increased surface roughness improves the overall biointegration of Ti-based implants through osteointegration and cell attachment [12, 14]. Biocompatibility is assessed by analyzing interfacial properties such as roughness and uniformity as well as biocorrosion susceptibility and biocorrosion rates. The biocorrosion tests were carried out in a simulated body fluid (Hank's Balanced Salt Solution, HBSS) and at physiological temperature.

Experimental section

Preparation of disk-shaped and wire-shaped specimens

The experimental work was done using wire-shaped and disk-shaped samples that were prepared from a commercially pure Ti wire (99.7%; Aldrich Chemical) of 0.81 mm in diameter and a commercially pure Ti foil (99.7% Ti; Alfa Aesar) of 1.0 mm in thickness. The commercially pure Ti has a density (ρ) of 4.51 g cm^{-3} and an equivalent weight (EW) of 16.00 g [15]. The disk-shaped samples were of 13 mm in diameter and were spot-welded to a Ti wire for electrical contact that was required for passivation and electrochemical studies. Such prepared disk-shaped electrodes were used in surface-chemical analysis and morphology studies. The wire-shaped samples were of 0.81 mm in diameter and ca. 10 mm in length. The end of the Ti wire was mechanically polished to obtain a flat tip [5]. The exact length of each sample was determined with a Vernier microscope. Each wire-shaped sample was connected to a copper wire for electrical contact and the connection was sealed with an epoxy resin and then protected with Teflon tape. Only the Ti wire was exposed to the medium in which experiments were carried out. Initial cleaning of all the Ti samples was done in hot acetone under reflux for 2 h. Samples were then micro-sandblasted with 90 μm alumina (Al_2O_3) using a Macro Cab micro-sandblaster (Danville Engineering Inc.), rinsed with demineralized water (Millipore) and sonicated in demineralized water for 5 min.

Electrochemical passivation

Electrochemical passivation of Ti samples was performed in an one-compartment electrochemical cell containing 7.5% (wt) aqueous NH_4BF_4 at $T = 298 \pm 3$ K. During electrochemical passivation, the sample was placed at a distance of ca. 10 cm from the counter electrode (Pt foil for the wire-shaped samples and Ti foil for the disk-shaped samples). An AC voltage (V_{AC}) was applied for a passivation time of $t_{pass} = 10$ s using a variable AC power supply (3 KVA AC Power Source Model 3001iM, California Instruments, San Diego, USA). The applied V_{AC} ranged from 10 to 50 V, with an interval of $\Delta V_{AC} = 10$ V, and its frequency (f) was kept at $f = 60$ Hz for all samples. Because the passivation proceeds with heat generation (resistive heating of the electrolyte solution) and gas evolution that can affect the quality of the passive layer, the electrolyte was thoroughly stirred and cooled using an

immersed cooling coil to ensure uniformity of the passive layer; this procedure allowed us to maintain the temperature within 3 °C of the room temperature [6, 10]. Subsequently, samples were carefully rinsed with demineralized water several times and sonicated for 5 min. This procedure guaranteed removal of any traces of the electrolyte as shown elsewhere [10]. In order to reduce exposure to the ambient and possible contamination, passivated specimens were prepared no more than 30 min before an analysis.

Surface analysis

Microscopic surface morphology was examined using a metallographic light microscopy (SEIWA Optical, Tokyo, Japan) at a magnification of 400×. The average surface roughness (R_a) before and after electrochemical passivation was analyzed using a stylus surface profiler (Dektak 8, Vecco, Tucson, USA) with a diamond stylus having a radius of 12.5 μm. A scanning electron microscope (SEM, Amray, Model 1380) was employed to examine the surface morphology in the sub-micron range.

Electrochemical characterization

Potentiodynamic polarization tests were carried out in a standard three-compartment electrochemical cell using a Princeton Applied Research (PAR) 263A potentiostat. The working electrode was the Ti specimen of interest, the counter electrode was Pt gauze, and the reference electrode was a saturated calomel electrode (SCE, Aldrich Chemical). The electrolyte, HBSS, was de-aerated with ultra-high purity N_2(g) for 1 h before electrochemical characterization; the cell was kept at a constant temperature of $T = 310 \pm 0.5$ K (or 37.0 °C) using a Haake W13 water bath and a Haake D1 thermostat to simulate the human body temperature. ASTM international standards [16–20] were carefully followed when performing potentiodynamic tests and their analysis yielded corrosion characteristics. PAR PowerCorr software package was used for data acquisition and analysis. Corrosion rates were calculated using Tafel extrapolation in the ±0.05 V range of the corrosion potential (E_{corr}) [6]. The reported corrosion rates and corrosion potentials are the mean values of at least three reproducible measurements.

Results and discussion

Appearance and surface morphology

Colored passive films were successfully formed on the Ti disk- and wire-shaped samples. The colors obtained are reproducible for all values of V_{AC}; the coloration obtained at a given V_{AC} is not shown because these results were previously reported elsewhere [5, 6, 10, 11]. The hues obtained by applying V_{AC} ranging from 10 to 50 V include royal blue, turquoise, plum, yellow, and brass, all with a matte finish that originates from the roughening effect of the micro-sandblasting pretreatment. As determined in our previous research, the thickness of the passive layers formed at $V_{AC} = 10$–50 V is in the sub-micrometer range and the greater the value of V_{AC}, the thicker the passive layer [6, 10]. Precise determination of the thickness of passive layers on surfaces roughened by micro-sandblasting is experimentally very difficult. However, the coloration obtained at a given V_{AC} can be used to estimate their thicknesses. Control of the material's coloration is important for medical and dental implants as a subcutaneous device may be visible through the skin. Light microscopy images were acquired for each sample at a 400× magnification. The images shown in Fig. 1 reveal uniform and defect-free surfaces. Some samples (e.g., Fig. 1h) showed evidence of contamination in the form of a particle (the feature is marked with a rectangle) embedded in the passive layer. The morphology of the samples and the distribution of the particles were further investigated using SEM.

Figure 2 presents a set of SEM micrographs of Ti disk-shaped samples, which were micro-sandblasted (a), and micro-sandblasted and passivated (b–f) at various V_{AC} values in the 10–50 V. These micrographs reveal rough surfaces having similar textures regardless of the applied V_{AC} value. They also reveal the presence of alumina (Al_2O_3) grains embedded in the surface as confirmed by energy-dispersive X-ray spectroscopy (EDX) measurements. They originate from the micro-sandblasting pretreatment and are larger in size than the grains of the Ti substrate. It is important to add that particles such as those visible in Fig. 2 were never observed when the samples were pretreated either by mechanical polishing or by chemical etching [5, 6].

Figure 3 shows an SEM image of the Ti sample pretreated using micro-sandblasting and passivated at $V_{AC} = 50$ V (main image) and an SEM image of as-received Al_2O_3 grains (inset). The main image demonstrates that the Al_2O_3 particles (emphasized using dashed-line rectangles) are randomly distributed and cover a small fraction of the entire surface. A comparison of the size of the as-received Al_2O_3 particles (their average size is specified by the manufacturer to be 90 μm) and the embedded Al_2O_3 particles in the Ti substrate indicates that the latter are significantly smaller due to mechanical breakdown during the sandblasting process. It is reasonable to conclude that the colored Ti remains the predominant phase after the micro-sandblasting pretreatment. It is interesting to observe that these Al_2O_3 particles survive

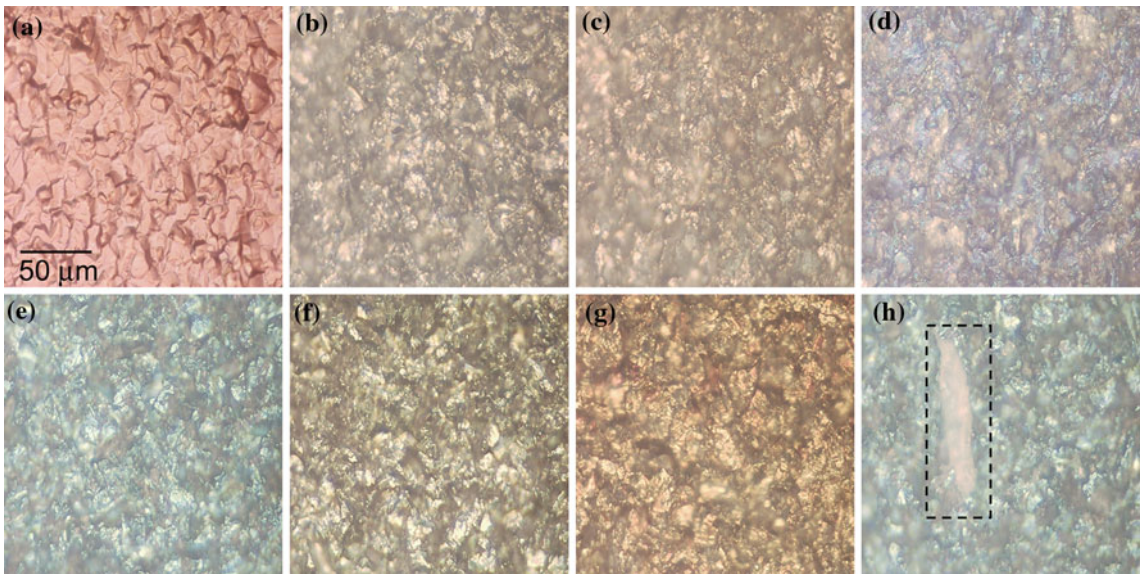

Fig. 1 Surface micrographs of eight different samples examined by light microscopy at a magnification of ×400. **a** As-received sample; **b** micro-sandblasted sample; **c** micro-sandblasted and passivated at $V_{AC} = 10$ V sample; **d** micro-sandblasted and passivated at $V_{AC} = 20$ V sample; **e** micro-sandblasted and passivated at $V_{AC} = 30$ V sample; **f** micro-sandblasted and passivated at $V_{AC} = 40$ V sample; **g** micro-sandblasted and passivated at $V_{AC} = 50$ V sample; and **h** micro-sandblasted and passivated at $V_{AC} = 30$ V sample with an embedded particle of Al_2O_3

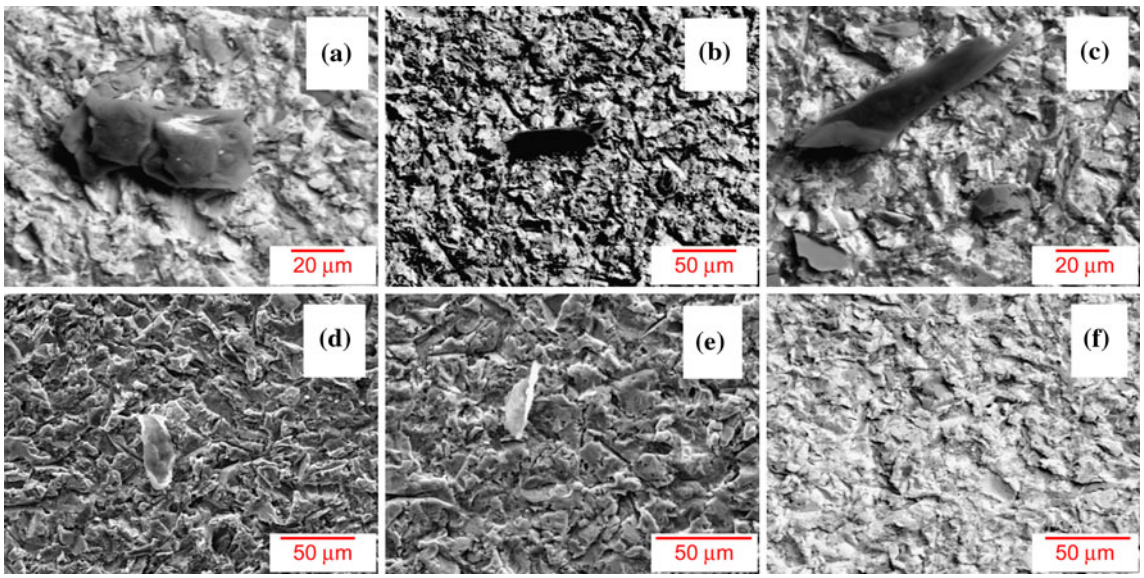

Fig. 2 SEM micrographs of micro-sandblasted (**a**) and micro-sandblasted and passivated Ti sample (**b–f**) at different V_{AC} values. **b** $V_{AC} = 10$ V; **c** $V_{AC} = 20$ V; **d** $V_{AC} = 30$ V; **e** $V_{AC} = 40$ V; and **f** $V_{AC} = 50$ V

extensive sample rinsing, sonication, and passivation. Descaling with hot and concentrated sodium hydroxide (NaOH) or with concentrated nitric acid (HNO_3) is a common procedure for removing alumina [21], but it was found ineffective in removing the Al_2O_3 particles. These results indicate that the Al_2O_3 particles are strongly embedded in the passive layers and remain mostly unaffected even after the exposure to strongly alkaline or acidic aqueous media. This observation is very important because it suggests that the alumina particles will remain in the surface of a dental or medical implant that has been pretreated by micro-sandblasting. Consequently, these particles may affect biocompatibility and surface roughness, and as such should be considered in further studies.

Stylus profilometry was employed to study the surface morphology of the micro-sandblasted Ti specimens before and after passivation, and to examine whether the roughness brought about by the micro-sandblasting pretreatment

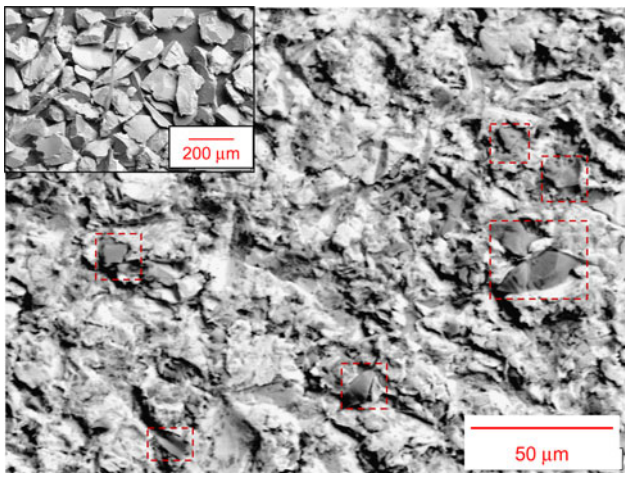

Fig. 3 SEM image of the Ti sample pretreated using micro-sandblasting and passivated at $V_{AC} = 50$ V (*main image*), and an SEM image of as-received Al_2O_3 particles (*inset*)

was uniform. Figure 4 shows three-dimensional (3D) topography for four samples that are representative of the overall trend (the detailed description of part figures are explained in the figure caption). In all cases, the profiles show random valleys and hills that create a rough surface, and the sample topography is found to be uniform. The average distance from the bottom of a valley to the top of a hill depends on the sample's pretreatment and is 11 ± 1 µm in the case of sample A, 15 ± 1 µm in the case of sample B, 13 ± 1 µm in the case of sample C, and 10 ± 1 µm in the case of sample D.

In addition to provide information about 3D surface topography, stylus profilometry can also be used to calculate the average surface roughness (R_a) which is simply the arithmetic average deviation of the surface from the mean level as expressed by Eq. 1:

$$R_a = \frac{1}{L} \int_{x=0}^{x=L} |y| \, dx, \tag{1}$$

where L is the scan length in the x direction (horizontal) and y is the vertical deviation of the surface from the mean height. Table 1 shows the values of R_a for the micro-sandblasted Ti samples before and after passivation. The value of R_a for the as-received and degreased Ti sample was determined to be 0.55 ± 0.09 µm. The values of R_a for the micro-sandblasted samples are consistently in the $0.85–1.10 \pm 0.35$ µm range. Micro-sandblasting increases the average roughness by 54–100%, as compared to the unmodified Ti sample ($R_a = 0.55 \pm 0.09$ µm). The values of R_a for the micro-sandblasted and passivated samples are in the $0.87–1.06 \pm 0.10$ µm range; they do not reveal any trend that could be related to the magnitude of V_{AC}. We observe that within experimental uncertainty electrochemical passivation hardly modifies the average surface roughness. Our results indicate that the average peak-to-valley distance does not change very much for the unmodified versus modified surfaces. However, the average surface roughness increases considerably for the modified surfaces as compared to the as-received Ti. These

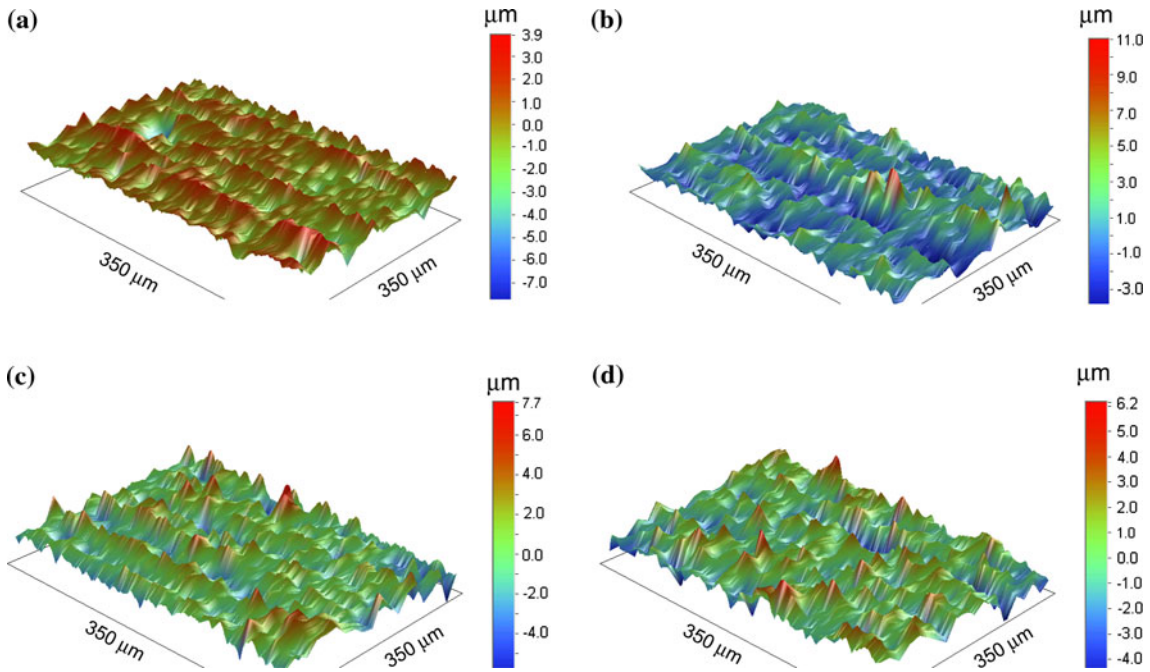

Fig. 4 Three-dimensional surface profiles for four Ti samples: **a** degreased and unmodified Ti; **b** Ti degreased and micro-sandblasted; **c** Ti degreased, micro-sandblasted and passivated at $V_{AC} = 10$ V; and **d** Ti degreased, micro-sandblasted and passivated at $V_{AC} = 30$ V

Table 1 Average surface roughness (R_a/μm) of micro-sandblasted Ti before and after electrochemical passivation at V_{AC} values

Treatment method	R_a (μm) after micro-sandblasting but before passivation	R_a (μm) after micro-sandblasting and passivation
Micro-sandblasted and passivated at $V_{AC} = 10$ V	0.97 ± 0.43	0.87 ± 0.19
Micro-sandblasted and passivated at $V_{AC} = 20$ V	1.10 ± 0.46	1.06 ± 0.41
Micro-sandblasted and passivated at $V_{AC} = 30$ V	0.98 ± 0.38	1.04 ± 0.26
Micro-sandblasted and passivated at $V_{AC} = 40$ V	1.01 ± 0.31	0.88 ± 0.24
Micro-sandblasted and passivated at $V_{AC} = 50$ V	0.85 ± 0.19	0.99 ± 0.31

The surface roughness of as-received Ti that serves as a reference is $R_a = 0.55 \pm 0.09$ μm

two finding might seem to be inconsistent. However, the value of R_a depends not only on the peak-to-valley distance but also on the density of peaks and valleys per unit surface area.

The pre-treatment method presented herein results in surface topography and R_a values which are in the range required to encourage biocompatibility of medical and dental implants. Research in the medical field demonstrates that the surface morphology of materials used for implants is an important factor that determines their successful integration within the human body. For example, uniformly roughened surfaces with R_a of 0.87 μm were shown to promote maximum cell adhesion [22]. Optimal surface roughness was also shown to promote osteointegration in laboratory studies of Ti surfaces roughened by micro-sandblasting. These roughened surfaces performed best at promoting the growth of osteogenic cells when compared with other surface pretreatment methods [23]. Currently, dental implants are inserted in a two-stage process: in the first stage, the foundation is put in place and are left to osteointegrate or "heal"; in the second stage, the actual implant is put in place. For most patients the first stage lasts 6 months before the procedure can be completed [12]. Micro-sandblasting, followed by electrochemical passivation may be a viable pre-treatment method for improving the surface properties of medical and dental implant materials to facilitate faster bioincorporation of the device.

Corrosion potential measurements

The measurements of E_{corr} can be used to evaluate the susceptibility of a material to undergo aqueous corrosion. Materials with high positive E_{corr} values are generally stable, while materials with large negative E_{corr} values are unstable and readily degrade through corrosion reactions [5]. The value of E_{corr} can be determined experimentally by measuring the open circuit potential (OCP) of the material as a function of time (t) and by extrapolating the value of OCP to $t \rightarrow \infty$ ($OCP_{t\rightarrow\infty} = E_{corr}$). Figure 5 shows a set of six OCP versus t transients for a micro-sandblasted Ti sample and for micro-sandblasted and passivated at a given V_{AC} Ti samples ($V_{AC} = 10$, 20, 30, 40, and 50 V). In order to simulate biocorrosion conditions, HBSS was used as the electrolyte and the measurements were carried out at the physiological temperature of $T = 310$ K (or 37 °C). The results show that a majority of the decrease of OCP takes place within the initial 600 s and reaches a steady-state value within 1 h. The limiting OCP value for $t = 3600$ s is accepted as E_{corr}, as there is very little further variation of OCP when the time is further extended. Figure 6 presents E_{corr} as a function of the applied V_{AC}; it also includes $E_{corr} = -0.67 \pm 0.010$ V for the micro-sandblasted Ti sample which serves as a reference. In general, the formation of passive layers increases the value of E_{corr} by ca. 0.20–0.48 V, depending on the applied V_{AC}, thus making the micro-sandblasted and passivated Ti samples less susceptible to corrosion in HBSS than the micro-sandblasted Ti. As V_{AC} increases from 0–30 V, E_{corr} increases from the initial value of -0.67 ± 0.010 to -0.22 ± 0.010 and then varies only slightly between -0.28 and -0.18 V for the passive layers formed at 40 and 50 V. In our previous articles [5, 6], we reported that as the magnitude of V_{AC} increases, the thickness of the passive layers also increases. The fact that E_{corr} increases most with $V_{AC} \leq 30$ V and almost levels off with $V_{AC} > 30$ V indicates that at $V_{AC} = 30$ V the passive layer reaches a thickness that offers the most effective protection against biocorrosion in HBSS. Elsewhere [5], we reported E_{corr} values for passive layers formed on etched Ti samples and also observed that an increase of V_{AC} increases E_{corr}, although those E_{corr} values were some 0.1–0.15 V greater than those reported in Fig. 6. This small difference of E_{corr} can be assigned to the micro-sandblasting which roughens the Ti surface and makes it more reactive as compared to chemically etched Ti.

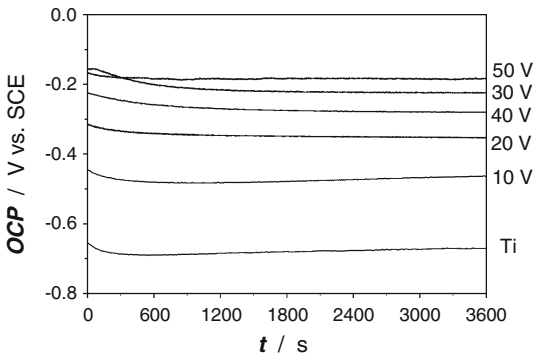

Fig. 5 OCP versus t transients obtained in HBSS and at $T = 310$ K for micro-sandblasted Ti and micro-sandblasted and passivated Ti at a given V_{AC}

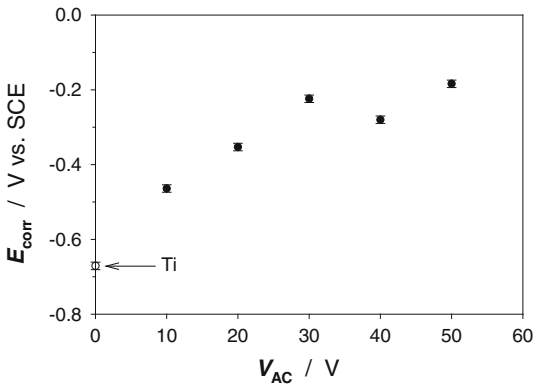

Fig. 6 Relation between E_{corr} in HBSS at $T = 310$ K and the V_{AC} required to form passive layers for the micro-sandblasted Ti. The value of E_{corr} for micro-sandblasted and non-passivated Ti is shown at $V_{AC} = 0$ V

Polarization curves and corrosion rates

Polarization curves for micro-sandblasted, and micro-sandblasted and passivated Ti samples were recorded in HBSS at $T = 310$ K (37 °C) and a scan rate of $s = 0.166$ mV s^{-1} to investigate the corrosion properties of these materials (Fig. 7). The polarization curve a refers to the micro-sandblasted Ti sample, while the polarization curves b–f are for the micro-sandblasted and passivated Ti samples. The inset in polarization curve b shows the methodology of determining E_{corr} and the corrosion current density (j_{corr}) by extrapolation of the two linear regions (within ca. 50 mV) of the lowest value of log j; the intercept of these two linear regions yields E_{corr} and log j_{corr}.

All the six polarization curves reveal the same common features: (i) a hydrogen (cathodic) region and an active (anodic) region (marked as "H region" in Fig. 7a); (ii) a poorly defined transition from the active to the passive region (marked in "A–P trans" in Fig. 7a); (iii) a flat quasi-passive region (marked as "Q–P region" in Fig. 7a) that resembles a passive region and has a passive current density (j_{pass}) value in the 10^{-6}–10^{-7} A cm^{-2} range; it is referred to as quasi-passive region because its shape resembles a passive region but the value of j_{pass} does not decrease significantly as compared to the active–passive transition; and (iv) a sudden increase of j by one to two orders of magnitude at ca. 1 V and another almost flat region with a small hump (marked as "j-IN region" in Fig. 7a). As compared to the polarization curve for micro-sandblasted Ti (Fig. 7a), the polarization curves for micro-sandblasted and passivated Ti (Fig. 7b–f) show less defined features and an overall reduction in the current density and its range of values. The consequence of the reduction of j in the passive-like region is an overall lower corrosion rate. The values of E_{corr} determined on the basis of polarization curves are −0.70 for micro-sandblasted Ti, and 0.18, −0.23, −0.32, −0.38, and −0.41 V for micro-sandblasted and passivated Ti at $V_{AC} = 10$, 20, 30, 40, and 50 V, respectively. These values differ from those reported in Fig. 6 and the origin of this difference lie in the nature of the experimental procedure. Specifically, in the case of the OCP measurements, the sample is immersed in the electrolyte solution and its OCP is monitored as a function of time. Importantly, the sample has not undergone any prior polarization and the OCP measured is characteristic of the processes spontaneously occurring at the electrode. In the case of polarization curves, the transients start at a negative potential, typically located between −1.0 and −0.5 V, and is scanned linearly to the upper limit of 3.0 V. The samples are initially exposed to negative potentials at which the following processes can take place: (i) electrolytic H_2(g) generation; (ii) partial reduction of the passive layer on Ti; and (iii) possible hydrogen absorption into Ti. The processes (ii) and (iii) have the ability to modify the electrode material such that it is no longer just micro-sandblasted and passivated Ti. Thus, following the cathodic polarization, the passive layer most likely has a different composition (partially reduced Ti oxide), possibly a Ti hydride forms in the near-surface region, and the protective passive layer is no longer compact and may have cracks. Consequently, the value of E_{corr} determined on the basis of polarization curves are expected to have different values than those determined using OCP measurements.

Cyclic polarization curves can be interpreted qualitatively to explain a metal's susceptibility to pitting or crevice corrosion [5, 15]. When a metal is highly susceptible to this type of corrosion, the polarization curve at the upper potential limit will show a well-defined hysteresis loop in the reverse scan [19]. An analysis of the results shown in Fig. 7 reveals the absence of a closed hysteresis loop in the polarization curves. Therefore, we can conclude that the micro-sandblasted Ti and micro-sandblasted and passivated Ti have low susceptibility to pitting or crevice corrosion in HBSS.

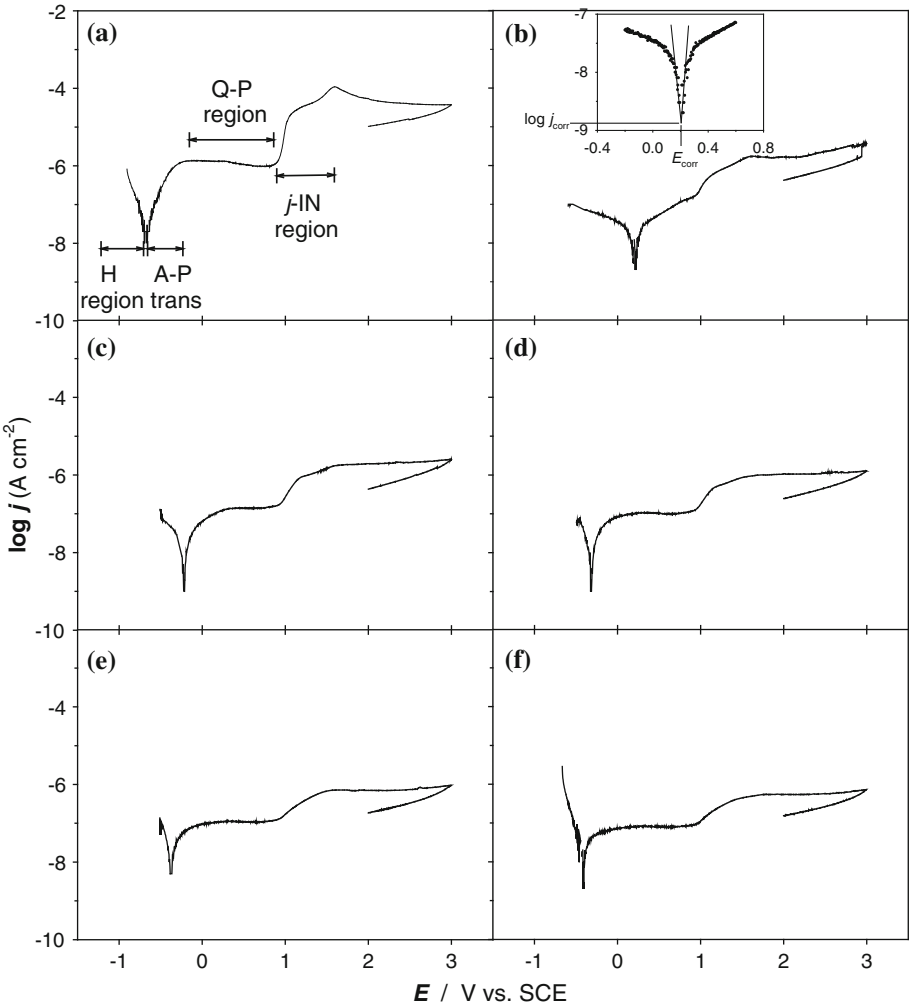

Fig. 7 Polarization curves for micro-sandblasted, and micro-sandblasted and passivated Ti samples recorded in HBSS at $T = 310$ K at a scan rate of $s = 0.166$ mV s^{-1}. **a** Micro-sandblasted Ti sample, **b–f** micro-sandblasted and passivated Ti samples at $V_{AC} = 10$, 20, 30, 40, and 50 V, respectively. The *inset* in the polarization curve B shows the methodology of determining the corrosion potential (E_{corr}) and the corrosion current density (j_{corr})

Corrosion rates (CR) can be obtained from polarization curves by applying the Stern–Geary equation, Eqs. 2 and 3:

$$\mathrm{CR} = \frac{3.27\, j_{\mathrm{corr}}\ \mathrm{EW}}{d} \tag{2}$$

$$j_{\mathrm{corr}} = \frac{\beta_{\mathrm{A}}\ \beta_{\mathrm{C}}}{2.3\ R_{\mathrm{p}}(\beta_{\mathrm{A}} + \beta_{\mathrm{C}})}, \tag{3}$$

where EW is the equivalent weight of the metal and d is its density, j_{corr} is the corrosion current density at E_{corr} (see the inset of Fig. 7b), R_p is the polarization resistance, β_A is the anodic Tafel slope and β_C is the cathodic Tafel slope. The value of R_p was determined on the basis of polarization resistance curves in the potential range (E_{corr} −0.20; E_{corr} +0.20). Figure 8 shows the average of three CR values for each passive film as a function of the applied V_{AC}; we also show the CR value of micro-sandblasted Ti that serves as a reference. The passive films formed at all the V_{AC} values reported were successful in reducing corrosion rates in HBSS. The film formed at $V_{AC} = 10$ V has the most significant reduction of CR that is 0.049 μm year^{-1} in HBSS; it contrasts favorably to CR for the micro-sandblasted Ti that is 0.735 μm year^{-1}. This represents approximately 15-fold reduction in the corrosion rate under the experimental conditions reported above. There is a gradual increase of CR with the magnitude of V_{AC} and the relationship is close to linear for $V_{AC} = 10$, 20, and 30 V.

The E_{corr} values (Fig. 6) determined on the basis of OCP versus t measurements reveal that the thick passive layers formed at $V_{AC} \geq 30$ V offer the most protective surface against corrosion in HBSS. On the other hand, the CR values (Fig. 8) determined on the basis of polarization curves show that the passive layer formed at $V_{AC} = 10$ V has the lowest value of j_{corr}, thus CR. These two observations seem to contradict each other and need to be discussed. Above, we have discussed the nature of the two experimental methods: (i) in the case of the OCP measurements, the sample is immersed in the electrolyte solution and its OCP is monitored as a function of time; the sample has not undergone any prior polarization; (ii) in the case of polarization curves, the transients start at a negative potential and end at a positive potential; the initial exposure to negative potentials might irreversibly modify the

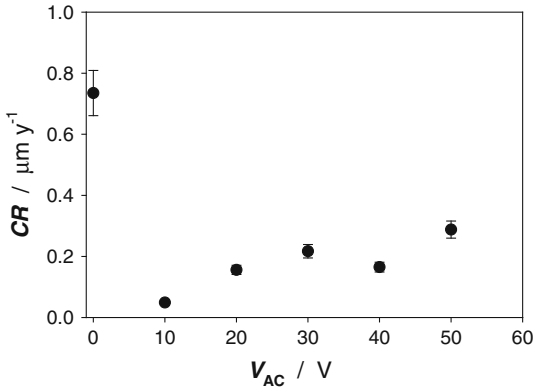

Fig. 8 CR for micro-sandblasted and passivated Ti as a function of V_{AC} required to form them. The value of CR for micro-sandblasted and non-passivated Ti is shown at $V_{AC} = 0$ V

sample. Therefore, the values of E_{corr} determined through OCP measurements are more reliable and, consequently, could be applied as a guideline in any potential practical application of the AC voltage-formed protective layers on micro-sandblasted Ti because any implant is very unlikely to be exposed to any strong cathodic polarization before implantation.

Conclusions

Electrochemically formed passive layers on micro-sandblasted Ti are uniform, crack free, and exhibit well-defined and reproducible coloration that is related to the magnitude of V_{AC} required to form them. The morphology of the micro-sandblasted surface before passivation is rough and non-uniform. Electrochemical passivation does not have a significant effect on the average surface roughness of the sample. The unique surface morphology achieved by the application of micro-sandblasting might facilitate the incorporation of an implant through cell adhesion and osteointegration. The measurements of E_{corr} show that the stability of micro-sandblasted Ti increases after electrochemical passivation. All passive layers offer a significant reduction of the corrosion rate as compared to micro-sandblasted and non-passivated Ti. The electrochemical passivation might offer a fast and easy way to decrease the corrosion rate of Ti within the human body. Thus, the combination of micro-sandblasting and electrochemical passivation may be beneficial to the overall biocompatibility of Ti.

Acknowledgement We acknowledge the National Science and Engineering Research Council (NSERC) of Canada, the Canada Foundation for Innovation, Ministry of Research and Innovation of Ontario, and Queen's University for their financial support as well as the Department of Geological Sciences for the facilities used in this study.

References

1. Clark RJH (1968) The chemistry of titanium and vanadium. Elsevier, New York
2. Tschernitschek H, Borchers L, Geurtsen W (2005) Quintessence Int 36:523
3. ADA Council on Scientific Affairs (2003) J Am Dent Assoc 134:347
4. Williams D (ed) (1990) Concise encyclopedia of medical & dental materials. Pergamon Press, Toronto
5. Zhao B, Jerkiewicz G (2006) Can J Chem 84:1132
6. Hrapovic S, Luan BL, D'Amours M, Vatankhah G, Jerkiewicz G (2001) Langmuir 17:3051
7. Solar RJ (1979) In: Syrett A (ed) Corrosion and degradation of implant materials. American Society for Testing and Materials, STP 684, Philadelphia, p 259
8. Lide DR (1993) CRC handbook of chemistry and physics, 74th edn. CRC Press, Boca Raton
9. Fukuzuka T, Shimogori H, Satoh H, Kamikubo F (1980) In: Kimura H, Izumi O (eds) Titanium '80-Science and Technology Proceedings of the Fourth International Conference on Titanium, Kyoto
10. Jerkiewicz G, Strzelecki H, Wieckowski A (1996) Langmuir 12:1005
11. Jerkiewicz G, Zhao B, Hrapovic S, Luan BL (2008) Chem Mater 20:1877
12. Brunette DM, Tengvall P, Textor M, Thomsen P (eds) (2001) Titanium in medicine material science, surface science, engineering, biological responses and medical applications. Springer, New York
13. Munro A, Cunningham MF, Jerkiewicz G (2010) ACS Appl Mater Interfaces: 2:854
14. van Noort R (1987) J Mater Sci 22:3801. doi:10.1007/BF01133326
15. Schutz RW, Thomas DE, Davis JR, Destefani JD, Frissell HJ, Crankovic GM (eds) (1987) ASM Handbook, vol 13, 9th edn. ASM International, Materials Park
16. ASTM G5-94 (2004) Standard reference test method for making potentiostatic and potentiodynamic anodic polarization measurements ASTM, Philadelphia
17. ASTM G59-97 (2003) Standard Test Method for Conducting Potentiodynamic Polarization Resistance Measurements ASTM, Philadelphia
18. ASTM G102-89 (2004) Standard Practice for Calculation of Corrosion Rates and Related Information from Electrochemical Measurements ASTM, Philadelphia
19. ASTM STP 727 (1981) Cyclic Polarization Measurements-Experimental Procedure and Test Data ASTM, Philadelphia
20. ASTM G3 (2004) Standard Practice for Conventions Applicable to Electrochemical Measurements in Corrosion Testing ASTM, Philadelphia
21. Parthasaradhy NV (1989) Practical electroplating handbook. Prentice-Hall, New Jersey
22. Bowers KT, Keller J, Randolph B, Wick D, Michaels C (1992) Int J Oral Maxillofac Implant 7:302
23. Boyan BD, Batzer R, Kieswetter K, Liu Y, Cochran DL, Szmuckler-Moncler S, Dean DD, Schwarts Z (1998) Biomed Mater Res 39:77